WIDEBAND FREQUENCY EXCURSIONS IN COMPUTED AM-FM IMAGE MODELS

J.P. Havlicek †, *D.S. Harding* ‡, *N.D. Mamuya* †, *and A.C. Bovik* ‡

† School of Electrical & Computer Eng., University of Oklahoma, Norman, OK 73019
‡Center for Vision and Image Sciences, University of Texas, Austin, TX 78712

ABSTRACT

We examine two paradigms for computing multicomponent AM-FM image models. In *channelized components analysis*, estimates for one AM-FM component are extracted from each channel of a multiband filterbank. *Tracked multi-component analysis* represents an image using fewer components by tracking the estimated modulating functions of each component across filterbank channels. While both approaches work well for synthetic images, they have difficulty with natural images that contain phase discontinuities. We show that phase discontinuities lead to wideband frequency excursions that make the computation of AM-FM models difficult and can also severely degrade the quality of image reconstructions obtained from the models. We use postfilters to ameliorate the effects of the frequency excursions and compute AM-FM models for two natural images.

I. INTRODUCTION

Intense recent research has been focussed on modelling images as finite sums of AM-FM functions [1–5]. Whereas the 2D Fourier transform represents an image as a linear composition of sinusoidal gratings each having constant amplitude and frequency, AM-FM functions are nonstationary sinusoids admitting instantaneous amplitudes and phases that are permitted to contain smooth, wideband variations across the image domain. Thus, each individual component in a computed AM-FM image representation is capable of capturing significant nonstationary structure. In principle, therefore, it should be possible to represent many natural images accurately using only a small number of computed AM-FM components.

Computed AM-FM image models are of great practical interest for at least two reasons. First, the inherently nonstationary character of the approach tends to lead naturally to representations *in terms of* local nonstationary image structures. This facilitates the analysis of images in terms of their nonstationarities, which are often information rich. For example, computed AM-FM image models have been used successfully for image segmentation, stereopsis, and 3D surface reconstruction [1, 6–8]. Second, while computed AM-FM models are inherently lossy, we have demonstrated that high-quality image reconstructions can often be obtained from the estimated amplitude and frequency modulations in a computed AM-FM representation [5]. Frequently, the modulating functions in such a representation are exceedingly smooth; we are currently investigating techniques for *compressing* the computed modulations to develop AM-FM based image coding strategies.

A block diagram of the *Channelized Components Analysis*, or *CCA*, paradigm for computing multicomponent AM-FM image models is shown in Fig. 1. In CCA, the image is first analyzed with a linear multiband Gabor filterbank. Fig. 2 depicts the filterbank in the frequency domain. Estimated modulating functions for one image component are then computed from each filterbank channel response using the demodulation algorithms described in [4] and briefly in Section III. Thus, the number of components in a CCA AM-FM image representation is always equal to the number of channels in the multiband filterbank.

The block diagram of another computational paradigm called *Tracked Multicomponent Analysis*, or *TMCA*, is shown in Fig. 3. Like CCA, TMCA begins by analyzing the image with a multiband Gabor filterbank. The difference between the two approaches is that TMCA seeks to represent the image using a number of AM-FM components that is smaller than the number of filterbank channels. Thus, in TMCA, a single image component is permitted to lie in different filterbank channels at different points in the image. As described in [4], Kalman filters are used to track the AM-FM image components across the filterbank channel responses.

Both the CCA and TMCA approaches tend to

This research was supported in part by the Army Research Office under contract DAAH 049510494 and by the Air Force Office of Scientific Research under grant F49620-93-1-0307.

0-7803-4876-1/98/$10.00 © 1998 IEEE

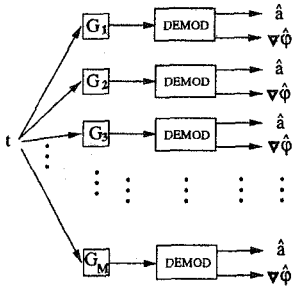

Figure 1: Block diagram of CCA, the Channelized Components Analysis paradigm.

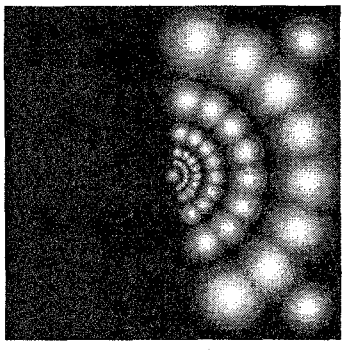

Figure 2: Frequency domain depiction of multiband Gabor filterbank.

work well when applied to synthetic images that do not conatain phase discontinuities. However, natural images and video may be expected to contain large numbers of phase discontinuities arising from a whole host of factors including occlusions, surface discontinuities, deformations and defects in surface topology, surface reflectance, shadows, specularities, and noise [1]. We have observed that natural images containing phase discontinuities tend to be problematic for the CCA and TMCA approaches. The computed modulations often exhibit large, localized amplitude spikes that severely degrade the quality of the reconstrutions delivered by both approaches, as well as wideband frequency excursions that can cause TMCA to fail altogether.

In this paper, we discuss why phase discontinuities are problematic for CCA and TMCA. We show that the discontinuities generally lead to wideband frequency excursions which tend to be accompanied by large scale amplitude variations of the type we have observed experimentally. Finally, we develop postfilters to smooth the frequency excursions and to compute high-quality reconstructions of natural images from their computed AM-FM representations.

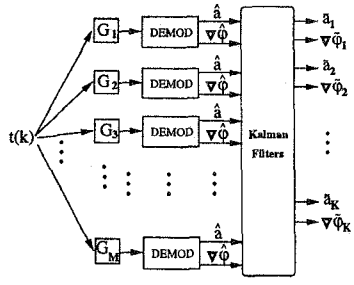

Figure 3: Block diagram of TMCA, the Tracked Multicomponent Analysis paradigm.

II. PHASE DISCONTINUITIES AND FREQUENCY EXCURSIONS

In both the CCA and TMCA paradigms, the instantaneous amplitude and frequency of each component in a multicomponent image are estimated from bandpass filterbank channel responses. In this section, we examine the nature of simple phase discontinuities and investigate their effects on the instantaneous frequency of a bandpass filtered AM-FM component. Suppose that

$$t_i(x,y) = a_i(x,y)\exp[j\varphi_i(x,y)] \qquad (1)$$

is one component of a multicomponent image $t(x,y)$. By definition, $a_i(x,y)$ and $\nabla\varphi_i(x,y)$ are the instantaneous amplitude and frequency of component $t_i(x,y)$. Suppose further that $g_m(x,y)$ is the impulse response of a 2D bandpass filter and that component $t_i(x,y)$ dominates the filter response

$$\begin{aligned} y_m(x,y) &= t(x,y) * g_m(x,y) \\ &\triangleq \vartheta_m(x,y)\exp[j\psi_m(x,y)], \end{aligned} \qquad (2)$$

where the symbol $\triangleq$ indicates that the second line of (2) defines ϑ_m and ψ_m. Then, under reasonable assumptions, it may be shown that the instantaneous frequency $\nabla\psi_m(x,y)$ of the response $y_m(x,y)$ closely approximates the true instantaneous frequency $\nabla\varphi_i(x,y)$ of the component $t_i(x,y)$ [4,9].

A. 1D Analysis

Note that the gradient operator ∇ operates independently in each dimension. Hence, in studying how the effects of phase discontinuities in $\varphi_i(x,y)$ are manifest in the instantaneous frequency, it suffices to consider the dimensions independently. For simplicity, we will therefore restrict the discussion in this section and in Section II.B to the one-dimensional case.

Consider the simplest instance of a single component 1D AM-FM signal that admits a phase discontinuity:

$$t(x) = \exp\left\{j\left[\Omega_0 x + \Upsilon u(x)\right]\right\}. \quad (3)$$

The phase discontinuity in $t(x)$ occurs at the point $x = 0$, where $\Upsilon \in [0, 2\pi]$ is the magnitude of the discontinuity and $u(x)$ is the unit step function. The instantaneous frequency of $t(x)$ is given by

$$\varphi'(x) = \Omega_0 + \Upsilon\delta(x), \quad (4)$$

where the Dirac delta $\delta(\cdot)$ is best interpreted in the sense of distributions. Thus, $\varphi'(x)$ is equal to Ω_0 everywhere except at the point $x = 0$, which is a set of Lebesgue measure zero.

If the signal (3) is applied to the 1D Gabor channel filter

$$g(x) = \frac{1}{\sqrt[4]{2\pi\sigma^2}} e^{-x^2/4\sigma^2} e^{j\Omega_0 x}, \quad (5)$$

then the filter response is given by

$$y(x) = t(x) * g(x) = \sqrt[4]{8\pi\sigma^2} e^{j\Omega_0 x} \times \left\{\left[1 - \Phi_e\left(\frac{x}{\sigma\sqrt{2}}\right)\right] + e^{j\Upsilon}\Phi_e\left(\frac{x}{\sigma\sqrt{2}}\right)\right\}, \quad (6)$$

where $\Phi_e(x)$ is the error function

$$\Phi_e(x) = \frac{1}{\sqrt{2\pi}} \int_{-\infty}^{x} e^{-\xi^2/2} d\xi. \quad (7)$$

The instantaneous frequency of the response (6) is given by

$$\psi'(x) = \Omega_0 + \frac{1}{2\sigma\sqrt{\pi}} e^{-x^2/4\sigma^2} \times \left\{\frac{\sin\Upsilon}{1 - 2(1 - \cos\Upsilon)\left[\Phi_e\left(\frac{x}{\sigma\sqrt{2}}\right) - \Phi_e^2\left(\frac{x}{\sigma\sqrt{2}}\right)\right]}\right\}. \quad (8)$$

Far away from the site of the discontinuity, $y(x)$ is effectively sinusoidal and

$$\lim_{x \to \pm\infty} \psi'(x) = \Omega_0. \quad (9)$$

With regards to the estimation of $\varphi'(x)$ at points other than $x = 0$, the remaining terms in (8) may be interpreted as errors induced by the presence of the phase discontinuity in $t(x)$ and by filtering.

Near the discontinuity we have that

$$\lim_{x \to 0} \psi'(x) = \Omega_0 + \frac{1}{\sigma\sqrt{\pi}} \tan\frac{\Upsilon}{2}, \quad (10)$$

and the instantaneous frequency of the filtered signal (6) generally contains a wideband excursion which may be of either sign. For values of Υ near π, this frequency excursion can be *unbounded* in magnitude. The support of the region over which the frequency excursion is significant is determined by the exponential factor $e^{-x^2/4\sigma^2}$ in (8), the rate of decay of which is in turn governed by the Gabor filter time constant σ. For filters admitting wide temporal support, the interval where the frequency excursion is significant can be large.

B. The Discrete Case

Images are almost always acquired and processed as discrete signals. Suppose that $t(k)$ is a discrete signal containing the samples of (3) and let $g(k)$ be a discrete Gabor filter equivalent to (5) with a half-peak bandwidth of one octave. Denote the filter response by $y(k) = t(k) * g(k)$. The frequency estimates obtained by applying the discrete frequency demodulation algorithms given in [5, 10, 11] to $y(k)$ exhibit excursions similar to those discussed above for the continuous case. In the discrete case, however, a closed form expression analogous to (8) cannot be obtained.

Consider a signal of the form (3) with $\Omega_0 = 3\pi/5$ rad/sec and $\Upsilon = 3\pi/4$. After sampling with respect to a unity sampling interval, the Hertzian equivalent to Ω_0 is $f_0 = 0.3$ cycles/sample. A half-octave discrete Gabor filter with center frequency 0.1 cycles/sample was applied to $t(k)$. The frequency estimates obtained by demodulating the filter response $y(k)$ are shown in Fig. 4(a), and exhibit a pronounced positive-going frequency excursion.

Similar results for a signal with $\Omega_0 = \pi/5$ rad/sec, $f_0 = 0.1$ cycles/sample, and $\Upsilon = 5\pi/4$ are given in Fig. 4(b) for a half-octave Gabor filter with center frequency equal to 0.1. In this case, the frequency estimates exhibit a negative-going excursion. Finally, Fig. 4(c) shows the frequency estimates obtained for a signal with $\Omega_0 = \pi/5$ rad/sec and $\Upsilon = 3\pi/4$, where f_0 is again equal to 0.1 cycles/sample. The Gabor filter center frequency was also 0.1.

C. General Discontinuities

Generally, the AM-FM components encountered in natural images and video are substantially more complicated than the signal (3). Nevertheless, the foregoing arguments can still be applied approximately to analyze the types of frequency excursions that may be expected to occur.

Consider the phase $\varphi_i(x, y)$ of the image component $t_i(x, y)$ in (1). For practical applications, we may assume that $\varphi_i(x, y)$ is finitely supported and

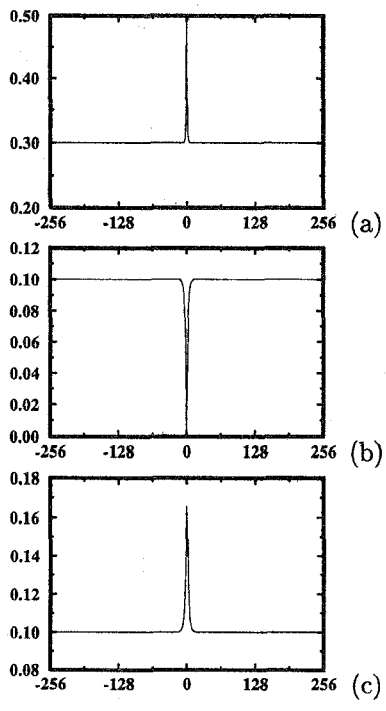

Figure 4: Discrete frequency estimates for a sinusoidal signal with frequency f_0 and a phase discontinuity of magnitude Υ. (a) $f_0 = 0.3$, $\Upsilon = 3\pi/4$. (b) $f_0 = 0.1$, $\Upsilon = 5\pi/4$. (c) $f_0 = 0.1$, $\Upsilon = 3\pi/4$.

bounded. Furthermore, since the image will almost always be sampled in practice, we assume that $\varphi_i(x,y)$ contains no isolated singularities or wild, erratic local behavior. Under these reasonable and practical assumptions, we may write $\varphi_i(x,y) = \theta(x,y) + \lambda(x,y)$, where $\theta(x,y)$ is continuous and $\lambda(x,y)$ is a sum of discontinuous steps.

The instantaneous frequency of $t_i(x,y)$ is then given by $\nabla\theta(x,y) + \nabla\lambda(x,y)$, where $\nabla\theta(x,y)$ exists as an ordinary function almost everywhere. The term $\nabla\lambda(x,y)$ will generally contain frequency excursions in the vicinity of the discontinuities. A detailed analysis of how these excursions are manifest in the filter response (2) is difficult and beyond the scope of this paper. However, to within errors inherent in the quasi-eigenfunction approximation given in [10], the instantaneous frequencies $\nabla\varphi_i(x,y)$ and $\nabla\psi_m(x,y)$ are *approximately* equal. Generally, frequency excursions in $\nabla\psi_m(x,y)$ may be expected to have increased spatial extent and be smeared as compared to those in $\nabla\varphi_i(x,y)$ as a consequence of filtering.

III. COMPUTATIONAL IMPLICATIONS

Consider once again that $t_i(x,y)$ in (1) is one component of a multicomponent image $t(x,y)$ and suppose this time that $t_i(x,y)$ dominates the response $y_m(x,y)$ in (2) at the point (x_0,y_0). It was shown in [9] that the instantaneous frequency $\nabla\varphi_i(x,y)$ may be estimated using the approximate demodulation algorithm

$$\begin{aligned}\nabla\varphi_i(x_0,y_0) &\approx \nabla\widehat{\varphi}_i(x_0,y_0) \\ &= \mathrm{Re}\left[\frac{\nabla y_m(x,y)}{j y_m(x,y)}\right]\Bigg|_{(x,y)=(x_0,y_0)} . \end{aligned} \quad (11)$$

The instantaneous amplitude $a_i(x,y)$ may then be estimated by

$$\begin{aligned} a_i(x_0,y_0) &\approx \widehat{a}_i(x_0,y_0) \\ &= \left|\frac{y_m(x,y)}{G_m[\nabla\widehat{\varphi}_i(x,y)]}\right|_{(x,y)=(x_0,y_0)} . \end{aligned} \quad (12)$$

In the neighborhood of a frequency excursion, both the demodulation algorithms (11) and (12) and their discrete equivalents discussed in [10] can suffer from large approximation errors. Furthermore, because Gabor filter frequency responses fall off rapidly outside the passband, modest to severe errors in the frequency estimates can cause the amplitude algorithm (12) and its discrete equivalent to deliver *absurdly* large estimates.

Even if frequency estimation errors do not occur, the fact that the instantaneous frequency can lie substantially outside the channel filter passband in the vicinity of an excursion can lead to numerical instability in the amplitude estimation, which again may result in absurdly large amplitude estimates. In either case, the erroneously large amplitude estimates can severely degrade the quality of the reconstructed images obtained from CCA and TMCA representations. Even more disastrous consequences can arise in TMCA, where frequency excursions often render the Kalman filters depicted in Fig. 3 unable to track individual image components at all. When this occurs, the approach fails altogether.

IV. POSTFILTERING SOLUTION

Our approach to ameliorating the effects of wideband frequency excursions is to process the modulating function estimates delivered by each filterbank channel with low-pass Gaussian postfilters having envelopes and bandwidths that are simply related to the channel filters. This postfiltering tends to suppress

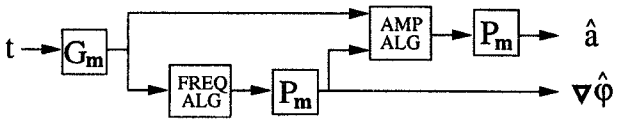

Figure 5: Postfiltered channel model.

excursions in the estimated frequency and to stabilize the amplitude estimation procedure. In TMCA, it also enables the Kalman filters to maintain component tracking across frequency excursions.

Each postfilter is most conveniently expressed in terms of a coordinate system that is rotated with respect to the orientation of the corresponding channel filter. Let γ_m be the orientation of the filter $g_m(x,y)$ and let $\beta = \gamma_m - \frac{\pi}{2}$. Define the rotated coordinates ζ_1 and ζ_2 by

$$\begin{bmatrix} \zeta_1 \\ \zeta_2 \end{bmatrix} = \begin{bmatrix} \cos\beta & \sin\beta \\ -\sin\beta & \cos\beta \end{bmatrix} \begin{bmatrix} x \\ y \end{bmatrix}. \qquad (13)$$

The impulse response of the postfilter for filterbank channel m is then given by

$$p_m(x,y) = \frac{1}{4\pi\kappa_1\kappa_2\sigma_m^2} \exp\left[-\frac{1}{4\sigma_m^2}\left(\frac{\zeta_1^2}{\kappa_1^2} + \frac{\zeta_2^2}{\kappa_2^2}\right)\right], \qquad (14)$$

where σ_m is the space constant of $g_m(x,y)$ and κ_1 and κ_2 are scaling factors that govern the relative amount of smoothing performed in the ζ_1 and ζ_2 directions.

The postfiltered channel model is shown in Fig. 5, where the initial frequency estimates computed using (11) are postfiltered. These postfiltered frequencies are then used in the amplitude algorithm (12), and the resulting amplitude estimates are themselves postfiltered.

V. EXAMPLES

The image *Raffia* is shown in Fig. 6(a). A reconstruction of the image obtained from a CCA AM-FM representation computed without postfiltering is shown in Fig. 6(b), and is of extremely low quality due to the presence of wideband frequency excursions. Numerous instances of absurdly large amplitude estimates are clearly visible and cause the dynamic range of the reconstructed image to grossly exceed the 8 bits used for display. The high-quality reconstruction given in Fig. 6(c) was obtained from a CCA AM-FM representation computed using postfilters.

Fig. 6(d) shows the image *Burlap*. A high-fidelity CCA reconstruction of the image computed with postfiltering is given in Fig. 6(e). Without postfiltering, the TMCA approach was unable to successfully track any components in the *Burlap* image due to the presence of frequency excursions. With the postfilters, 8 components were tracked and an 8-component TMCA representation was successfully computed. A reconstruction obtained from this representation is shown in Fig. 6(f), and is of remarkable quality for such a small number of components.

VI. CONCLUSION

Wideband frequency excursions generally cause substantial difficulties in the computation of multicomponent AM-FM image models. With the TMCA approach, the Kalman filters used to track image components across channels in the multiband filterbank often fail when frequency excursions are present. Even if tracking is maintained in the vicinity of an excursion, the wideband variations in the instantaneous frequency tend to make multiple image components difficult to resolve from one another. This typically results in severe cross-component interference that can produce significant errors in the computed modulating function estimates. For both the CCA and TMCA paradigms, frequency excursions lead to amplitude estimates that are absurdly large in magnitude. These erroneous amplitudes severely degrade the quality of the images reconstructed from the computed representations.

The fact that phase discontinuities generally produce wideband frequency excursions is significant since the phases of natural images may be expected to contain large numbers of discontinuities. Postfilters may be used to smooth the associated frequency excursions and ameliorate their deleterious effects. Furthermore, high-quality image reconstructions can be obtained from postfiltered AM-FM models.

VII. REFERENCES

[1] A. C. Bovik, M. Clark, and W. S. Geisler, "Multichannel texture analysis using localized spatial filters", *IEEE. Trans. Pattern Anal. Machine Intell.*, vol. 12, no. 1, pp. 55–73, January 1990.

[2] P. Maragos and A. C. Bovik, "Image demodulation using multidimensional energy separation", *J. Opt. Soc. Amer. A*, vol. 12, no. 9, pp. 1867–1876, September 1995.

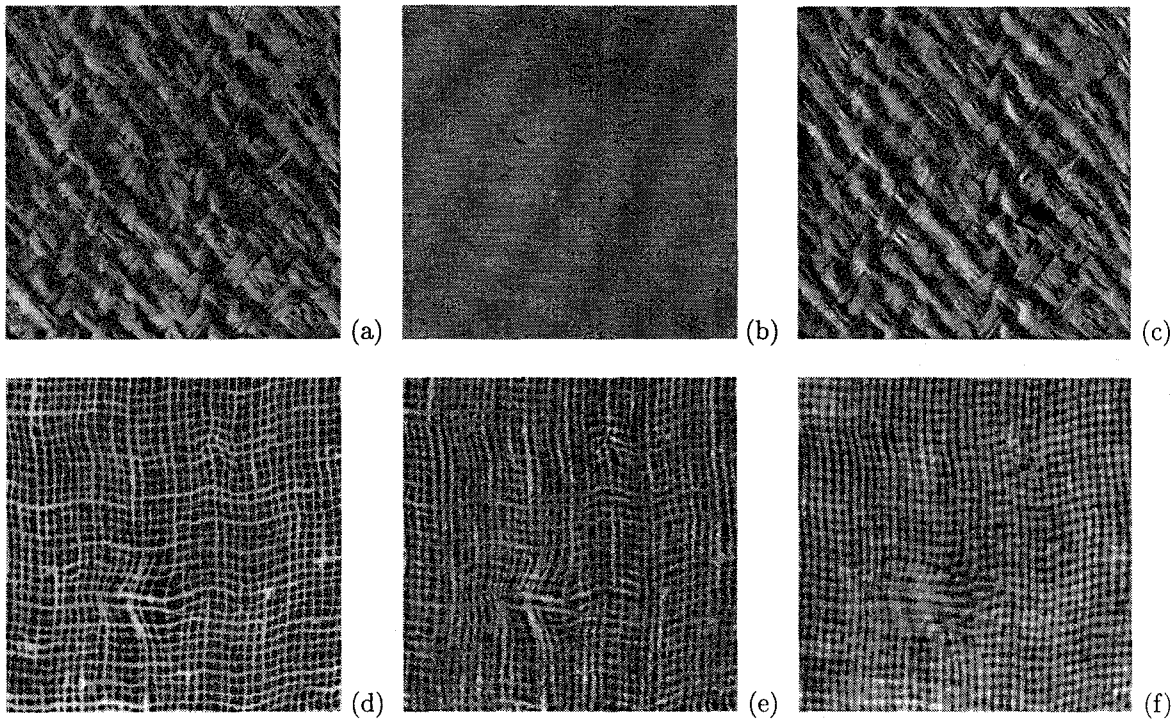

Figure 6: Examples. (a) *Raffia* image. (b) CCA reconstruction computed *without* postfiltering. (c) CCA reconstruction computed *with* postfiltering. (d) *Burlap* image. (e) Postfiltered CCA reconstruction. (f) Postfiltered TMCA reconstruction.

[3] B. Friedlander and J. M. Francos, "An estimation algorithm for 2-D polynomial phase signals", *IEEE Trans. Image Proc.*, vol. 5, no. 6, pp. 1084–1087, June 1996.

[4] J. P. Havlicek, D. S. Harding, and A. C. Bovik, "The multi-component AM-FM image representation", *IEEE Trans. Image Proc.*, vol. 5, no. 6, pp. 1094–1100, June 1996.

[5] J. P. Havlicek, D. S. Harding, and A. C. Bovik, "Extracting essential modulated image structure", in *Proc. 30th IEEE Asilomar Conf. Signals, Syst., Comput.*, Pacific Grove, CA, November 3-6, 1996, pp. 1014–1018.

[6] B. J. Super and A. C. Bovik, "Planar surface orientation from texture spatial frequencies", *Pattern Recog.*, vol. 28, no. 5, pp. 728–743, 1995.

[7] T. -Y. Chen and A. C. Bovik, "Stereo disparity from multiscale processing of local image phase", in *Proc. IEEE Int'l. Symp. Comput. Vision*, Coral Gables, FL, November 20-22, 1995.

[8] A. C. Bovik, N. Gopal, T. Emmoth, and A. Restrepo, "Localized measurement of emergent image frequencies by Gabor wavelets", *IEEE. Trans. Info. Theory*, vol. 38, no. 2, pp. 691–712, March 1992.

[9] J. P. Havlicek, A. C. Bovik, and P. Maragos, "Modulation models for image processing and wavelet-based image demodulation", in *Proc. 26th IEEE Asilomar Conf. Signals, Syst., Comput.*, Pacific Grove, CA, October 26-28, 1992, pp. 805–810.

[10] J. P. Havlicek, D. S. Harding, and A. C. Bovik, "Discrete quasi-eigenfunction approximation for AM-FM image analysis", in *Proc. IEEE Int'l. Conf. Image Proc.*, Lausanne, Switzerland, September 16-19, 1996, pp. 633–636.

[11] A. C. Bovik, J. P. Havlicek, D. S. Harding, and M. D. Desai, "Limits on discrete modulated signals", *IEEE Trans. Signal Proc.*, vol. 45, no. 4, pp. 867–879, April 1997.